Effects of Cellulose Nanowhiskers on Mechanical, Dielectric, and Rheological Properties of Poly (3-hydroxybutyrate-co-3-hydroxyvalerate)/Cellulose Nanowhisker Composites

ARTICLE *in* INDUSTRIAL & ENGINEERING CHEMISTRY RESEARCH · FEBRUARY 2012

Impact Factor: 2.59 · DOI: 10.1021/ie2023367

I&EC research
Industrial & Engineering Chemistry Research

Article

pubs.acs.org/IECR

Effects of Cellulose Nanowhiskers on Mechanical, Dielectric, and Rheological Properties of Poly(3-hydroxybutyrate-*co*-3-hydroxyvalerate)/Cellulose Nanowhisker Composites

Elena Ten,[†] David F. Bahr,[‡] Bin Li,[‡] Long Jiang,*[,§] and Michael P. Wolcott*[,†]

[†]Composite Materials and Engineering Center, PO Box 641806, Washington State University, Pullman, Washington 99164-1806, United States

[‡]School of Mechanical and Materials Engineering, PO Box 642920, Washington State University, Pullman, Washington 99164-2920, United States

[§]Department of Mechanical Engineering, PO Box 6050, North Dakota State University, Fargo, North Dakota 58108, United States

ABSTRACT: The thermal, mechanical, dielectric, and dynamic mechanical properties of polymer nanocomposites strongly depend on nanoparticles' content and aspect ratio. In this study, poly(3-hydroxybutyrate-*co*-3-hydroxyvalerate) (PHBV)/cellulose nanowhisker (CNW) composite films with various CNW concentrations (0−4.6 wt %) were prepared by solution casting. Bulge, tensile, and dynamic mechanical tests showed that mechanical properties of the films increased with increasing CNW content until the content reached 2.3 wt %. Real permittivity of the composites also peaked at 2.3 wt % CNWs over a wide spectrum of frequencies (0.01−10^6 Hz). These property transitions occurring at 2.3% CNW content were due to the transition of CNW dispersion from homogeneous dispersion to agglomeration. Rheological results of the composites, however, indicated a transition point lower than 2.3%. This was attributed to the existence of a polymer−CNW network in the composite melt, which required no physical touching or geometrical overlapping between CNWs.

INTRODUCTION

Over the past few decades, interest in developing lignocellulosic fiber reinforced composites has grown enormously. Due to their abundance, high specific moduli (modulus over density), stiffness of about 100−143 GPa,[1−3] and high aspect ratio, cellulose nanowhiskers (CNWs) are found to be a good reinforcement agent for a wide variety of polymeric matrixes. CNWs are rod-shaped highly crystalline fibrils that naturally occur in many plants (e.g., wood, hemp, sugar beet, sisal, cotton, and ramie), bacteria, and sea animals (e.g., tunicin).

The most common method to harvest CNWs from natural fibers is sulfuric acid hydrolysis followed by centrifugation. The mechanism to isolate CNWs is to destroy and remove noncrystalline regions which are present between nanowhiskers through chemical reactions. Hydrolysis conditions such as temperature and time influence the size[4] and stiffness[5] of the resulting CNWs. The sulfuric acid treatment introduces sulfate groups to the surface of CNWs. The negative charges on the CNW surfaces lead to high stability of aqueous CNW suspension.[6] Therefore, water-soluble polymers are readily used to prepare CNW−polymer nanocomposites. For example, polyvinyl alcohol (PVOH),[7−10] poly(methyl vinyl ether-*co*-maleic acid) (PMVEMA) with poly(ethylene glycol) (PEG),[11] furfuryl alcohol,[12] poly(styrene-*co*-butyl acrylate),[13−16] and poly(styrene-*co*-hexyl acrylate) latex,[17] starch,[10,18−24] poly(oxyethylene) (PEO),[25,26] natural rubber,[27−30] and soy protein isolate[31,32] have been used as the matrix polymers for CNW reinforcement. CNWs have also been successfully incorporated into water-insoluble polymers such as polyethylene,[33−35] polypropylene,[35−37] polyvinyl chloride,[38] polyvinyl acetate,[39] polycaprolactone,[40] poly(lactic acid),[41−47] poly(L-lactide),[48] cellulose acetate,[49] PHA,[50] cellulose acetate butyrate (CAB),[51−54] waterborne polyurethane[55−58] and epoxy.[59−61] In these studies, the addition of CNWs significantly improved mechanical and other physical properties of the polymers, including tensile strength,[8,9,12,15,18,21,22,32,35,37,46−49,55] storage modulus,[7,8,10,12,14,25,36,37,40,46−48,60] water resistance,[11,19,21,32,33,56] transparency,[21,51] and barrier properties.[22,47] To the best of our knowledge, only two studies have been reported on poly(3-hydroxybutyrate-*co*-3-hydroxyvalerate) (PHBV)/CNW composites,[62,63] and they were reported by our group. Our study on this nanocomposite system revealed that the composites prepared by the solution casting method showed good CNW dispersion and good mechanical properties. However, melt processed (extrusion followed by injection molding) composites demonstrated reduced mechanical properties due to severe CNW agglomeration.[62] The strong nucleating effect of CNWs on PHBV led to significant improvement in both mechanical (e.g., Young's modulus, tensile strength, and toughness) and dynamic mechanical properties (e.g., storage modulus) after the addition of 5 wt % of CNW powder.[63]

Favier et al. were the first to explain the reinforcing effect of CNWs in polymer matrixes.[13] Formation of a mechanical percolation network was reported to be responsible for improvement of the mechanical properties. They investigated poly(styrene-*co*-butyl acrylate) latex/cellulose nanocrystal (tunicin)

Received: October 11, 2011
Revised: December 21, 2011
Accepted: January 15, 2012
Published: January 16, 2012

dx.doi.org/10.1021/ie2023367 | *Ind. Eng. Chem. Res.* 2012, 51, 2941−2951

composite films prepared by solution casting. They showed that the shear modulus G of the nanocomposites was improved over a wide temperature range above the glass transition temperature (T_g) of the matrix. The reason was ascribed to the whisker percolation network introduced by hydrogen bonding between neighboring whiskers. The presence of such a network was later confirmed by electrical measurements performed on nanocomposites containing CNWs that were coated with conductive polypyrrole.[64] Later, the percolation behavior of CNWs in polymer matrixes was extensively studied by other research groups.[65−70]

In this study, a solvent exchange method was used to transfer CNWs from water to *N*,*N*-dimethylformamide (DMF). This method avoided drying and redispersion of CNW powder and therefore could reduce the probability of CNW agglomeration. PHBV/CNW nanocomposites were prepared by solution casting. The effects of CNWs on the thermal, dielectric, mechanical, and rheological properties of the composites were studied. The dimensions of CNWs and their dispersion in the composites were studied. Based on their aspect ratio, the mechanical percolation threshold of the CNWs was estimated.

EXPERIMENTAL SECTION

Materials. PHBV with 12 mol % hydroxyvalerate (HV) was supplied by Metabolix Inc. Its weight-average molecular weight M_w was determined to be 65 116 g/mol using gel permeation chromatography (GPC Max VE2001, Viscotek). The glass transition temperature T_g was ca. −5 °C (by differential scanning calorimetry (DSC)). *N*,*N*-Dimethylformamide (DMF) and NaOH were obtained from Acros Organics (Atlanta, GA). Microcrystalline cellulose (MCC), which is derived from wood pulp and has a high content of crystalline cellulose, was obtained from Avicel (Type PH-102). Sulfuric acid (96 wt %) was purchased from J.T. Baker. PHBV was dried at 80 °C in a convection oven for 12 h prior to use.

CNW Preparation. Sulfuric acid was diluted to 64 wt % concentration. MCC (1 g per 9.8 mL of acid) was added and vigorously stirred at 44 °C for 2 h. Then the suspension was diluted to about one-tenth of its original acid concentration. The sulfuric acid in the suspension was gradually removed by repeated centrifugation (Sorvall, 5000 rpm for 5 min) until the supernatant was turbid. The supernatant was a stable CNW suspension which could resist centrifugal precipitation. The supernatant was collected and dialyzed against deionized water for 4−5 days to remove the remaining acid and other chemicals (dialysis tube from Spectrum Laboratories Inc., cutoff molecular weight 12 000−14 000). The supernatant was further neutralized with 1 wt % NaOH (if necessary) and concentrated to 2% CNW concentration using a Büchi Rotavapor (R-200) operating at 80 °C.

PHBV/CNW Nanocomposite Preparation. Various amounts of concentrated CNW suspension were added dropwise into 40 mL of DMF under continuous stirring. Water was evaporated from the mixture at 80 °C for 1 h (DMF boiling temperature 153 °C) to obtain a CNW/DMF suspension. Different amounts of PHBV were then dissolved in the suspension. Sonication treatment was applied to the solution for 5 min to facilitate CNW dispersion. The solution was casted on a clean glass substrate and evaporated overnight at 50 °C, resulting in PHBV/CNW transparent films with thicknesses ranging from 15 to 30 μm (measured by a digital micrometer). The DMF content of the films was measured to be less than 2 wt % through vacuum drying (at 80 °C for 24 h). The CNW content of the films was determined to be 0.5, 1.2, 2.0, 2.3, 2.9, 3.3, 3.6, 4.2, and 4.6 wt % (or 0.4, 1.0, 1.6, 1.8, 2.3, 2.7, 2.9, 3.4, and 3.7 vol %, respectively) using thermogravimetric analysis (TGA).

CHARACTERIZATION

Transmission Electron Microscopy (TEM). The morphology of CNWs was studied by a TEM (JEOL 1200 EX) operating at 100 kV. A drop of CNW suspension was introduced on a Formvar and carbon coated copper grid, and the water was naturally evaporated at ambient temperature. TEM images of CNWs were acquired without any sample staining. To study the morphology of the composite film, PHBV/CNW films were embedded in acrylic resin LR White (London Resin Company Ltd.) and cured at elevated temperature overnight. Thin sections of ∼50 nm were cut from the cured block with a diamond knife using a Reichert-Jung ultramicrotome. The sections were placed on carbon coated copper grids and were subsequently stained with 2 wt % uranyl acetate for 90 min.

Atomic Force Microscopy (AFM). Morphologies of CNWs and PHBV/CNW films were also studied by AFM. A drop of CNW suspension was deposited on freshly cleaved mica surfaces, and the AFM scan was performed after water was completely evaporated. The AFM tests were carried out in tapping mode using a Veeco Multimode AFM equipped with a NanoScope IIIa controller (Digital Instruments Inc.). Silicon tips (Digital Instruments Inc.) with a resonance frequency of ca. 330 kHz were used. The scan rate was 0.5 Hz.

Thermogravimetric Analysis (TGA). TGA was performed on a TA Instruments Q600 to determine the thermal stability of the PHBV/CNW films. Based on the percentage weight loss, CNW contents in the films were deduced. Approximately 5−10 mg of the composite was placed in an aluminum pan. After equilibrating at 25 °C for 5 min, the sample was heated to 600 at 20 °C/min under 100 mL/min N_2 flow. Three replicates were tested for each sample.

Polarized Optical Microscopy (POM). The crystallization behavior of neat PHBV and PHBV/CNW nanocomposites was studied by an Olympus BX51 POM equipped with a Linkam hot stage (THMS600/HFS91). PHBV/CNW films were heated to 220 °C between two glass slides and then equilibrated at this temperature for 10 min to eliminate any residual PHBV crystallization seeds.[71] The films were then quenched in liquid nitrogen to obtain complete amorphous samples. Isothermal crystallization of PHBV at 30 °C was examined by the POM, and the micrographs of the crystals were taken by an attached digital camera after 5 and 20 min of crystallization time, respectively.

Differential Scanning Calorimetry (DSC). Thermal transitions of the nanocomposites were examined by a Mettler Toledo DSC 822e under N_2 flow (80 mL/min) and liquid nitrogen controlled cooling. Samples were crimple-sealed in aluminum crucibles and heated from −50 to 200 °C at a heating rate of 10 °C/min (first heating scan), equilibrated at 200 °C for 2 min, cooled rapidly at 30 °C/min to −50 °C, equilibrated at −50 °C for 2 min, and then heated again to 200 at 10 °C/min (second heating scan). The first heating scan was performed to eliminate the sample's thermal history.

Rheology Test. A strain-controlled rheometer (RDA III, Rheometric Scientific) was used to measure dynamic rheological properties of PHBV/CNW composites. The measurements were performed at 175 °C using parallel plate

dx.doi.org/10.1021/ie2023367 | *Ind. Eng. Chem. Res.* 2012, 51, 2941−2951

geometry (25 mm diameter). The gap between the two plates was 0.5 mm. Samples were equilibrated at 175 °C for 5 min before tests. A strain sweep test was first performed to determine the linear viscoelastic region of the composites, and a shear strain of 0.6% was chosen for all subsequent frequency sweep tests. The frequency was varied from 1 to 500 rad/s.

Dynamic Mechanical Analysis (DMA). DMA was conducted in tension mode on a Tritec 2000 DMA at 1 Hz to examine thermal dynamic properties of the films. DMA samples (10 × 6.5 mm^2) were cut from the PHBV/CNW composite film. Dynamic strain sweep was first performed to determine the linear viscoelastic range of the samples. Then the samples were tested from −40 to +80 °C at 5 °C/min heating rate with a strain of 0.02%. Ten replicates were tested for each composite formulation.

Tensile Test. Dumbbell-shaped film specimens were prepared with a type IV (ASTM D638) sample cutter and tested according to ASTM D 638-91. Ten samples for each formulation were tested using an Instron 4466 (capacity 500 N) at a deformation rate of 5.08 mm/min. Tensile strain was recorded by an EIR laser extensometer (Model LE-05).

Bulge Test. Bulge testing is commonly used to the test mechanical performance of thin films. In this test, PHBV/CNW films were loaded by pressurized dry air and the deflection of the films was measured (Figure 1). Air pressure was applied

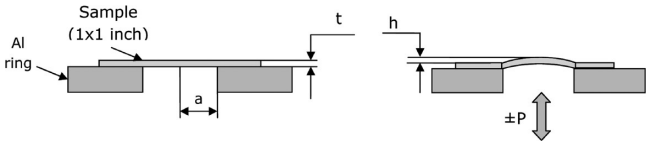

Figure 1. Schematic representation of the bulge test.

and varied by a Meriam pressure/vacuum variator. Film deflection was measured with a scanning laser vibrometer (Polytec OFV500). The pressure and deflection values were acquired using LabView software. Five replicates were tested for each specimen.

By fitting the curve of pressure versus deflection to a cubic polynomial, the Young's modulus of the film could be calculated from the slope of the polynomial using the model of circular membrane behavior under uniform pressure:[72]

$$P = \frac{8Et}{3a^4}h^3 + \frac{4t\sigma}{a^2}h \tag{1}$$

where P is the differential pressure, E is the modulus, t is the thickness of the film, a is the radius of the membrane (4.76 mm), h is the center deflection, and σ is the residual stress in the film determined by the deflection relationship at zero differential pressure:

$$\sigma = \frac{Pa^2}{4ht} \tag{2}$$

The experimental setup is depicted in Figure 1.

Dielectric Properties Measurement. Real (ε') and imaginary (ε'') parts of the dielectric constant and dielectric loss (tan δ) of the films were measured by an Alpha-N high resolution dielectric analyzer (Novocontrol Inc.) over 0.01−10^6 Hz frequency range at room temperature. Five replicates were tested for each composite formulation. Before measurements, samples were cleaned with acetone and dried at ambient temperature.

RESULTS AND DISCUSSION

Morphology of CNWs and PHBV/CNW Films. To confirm that CNWs formed a stable dispersion in DMF after solvent exchange, CNW/water and CNW/DMF suspensions were first observed between two crossed polarizers. If stable and homogeneous CNW suspensions were formed, flow birefringence could be observed due to the anisotropy of CNWs. Figure 2 shows that both suspensions exhibited strong

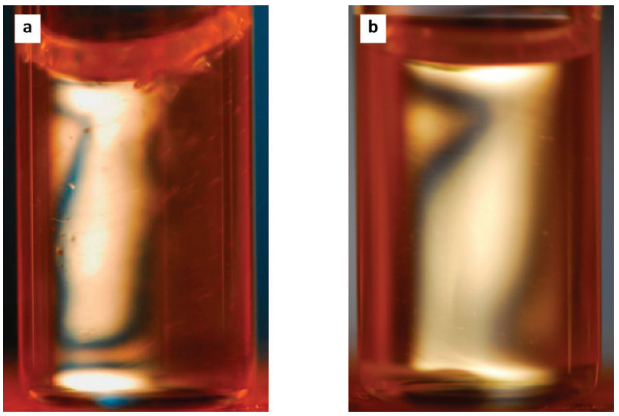

Figure 2. CNW suspensions showing flow birefringence between two crossed polarizers. CNW concentration is 0.9 wt % (a) in water and (b) in DMF.

flow birefringence, indicating that CNW dispersion remained stable and homogeneous in DMF after solvent exchange.

AFM images (topographic and phase) and a TEM micrograph of CNWs are shown in Figure 3. A wide distribution in CNW dimension is evident from both graphs. The dispersion of CNWs in the PHBV matrix is demonstrated by the TEM images shown in Figure 4. It is clear that CNWs were homogeneously dispersed in the PHBV matrix at low CNW concentration (Figure 4a). At higher concentrations (Figure 4b,c), agglomeration of CNWs became evident as indicated by the circles.

Due to the tip broadening effect in AFM micrographs, the dimensions (length and diameter) of CNWs were measured from their TEM micrographs. The TEM image in Figure 3c could not be used for the measurement because it was difficult to identify the ends of a single fiber. Therefore, all the measurements were performed on the CNWs in the PHBV/CNW composites (Figure 4). The CNW aspect ratio (length/diameter) of the fiber was determined based on the measurements of 300 individual whiskers using ImageJ software (National Institutes of Health). The average length and diameter were determined to be 221 ± 48 and 12.3 ± 4.0 nm, respectively. The average aspect ratio was calculated to be 18.01 ± 7.5.

An aspect ratio distribution histogram of CNW is shown in Figure 5. A log-normal distribution that is commonly used to describe particle size distribution was used to fit the histogram:

$$f(x) = \frac{\exp\left(-\frac{1}{2}\left(\frac{\ln(x)-\mu}{\sigma}\right)^2\right)}{x\sigma\sqrt{2\pi}} \tag{3}$$

where x is a random variable (in this case aspect ratio) with normal distribution; μ and σ are location and scale parameters,

dx.doi.org/10.1021/ie2023367 | Ind. Eng. Chem. Res. 2012, 51, 2941−2951

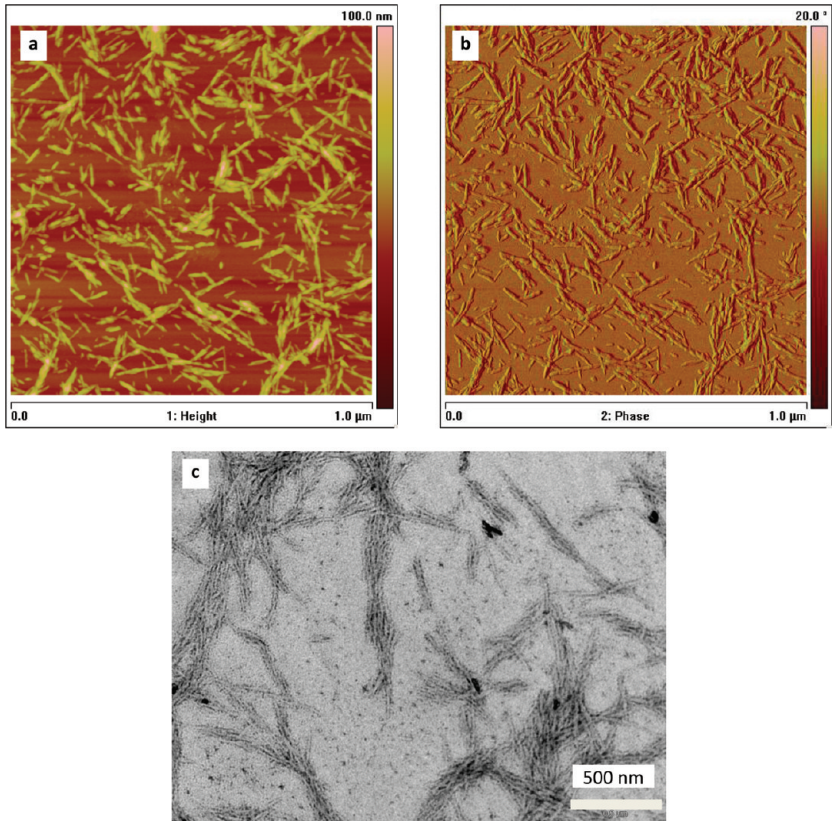

Figure 3. (a) AFM topographic image, (b) AFM phase image, and (c) TEM micrograph of CNWs. CNW samples were obtained by evaporating water from the aqueous suspension of CNWs.

respectively. μ = 2.7 and σ = 0.58 were obtained for the best fitting.

Therefore, the aspect ratio distribution can be described as

$$f(x) = \frac{\exp\left(-\frac{1}{2}\left(\frac{\ln(x) - 2.7}{0.58}\right)^2\right)}{0.58\sqrt{2\pi}\,x} \quad (4)$$

An average aspect ratio can be determined as

$$\frac{L}{d} = e^{\mu+\sigma^2/2} = 18.02 \quad (5)$$

This value is very close to the measured average aspect ratio. It should be recognized that this aspect ratio is most likely smaller than the actual value because CNWs were randomly oriented in the film. The measured fiber length in this situation was actually the projected fiber length, which was often smaller than the real fiber length. The measurements taken on unidirectionally aligned CNW composites should give CNW aspect ratios close to the actual values. This part of work has been done and will be reported in our next paper.

Thermal Properties. The thermal behavior of PHBV with respect to the CNW concentration was studied by DSC. The thermograms for the first cooling and the second heating scan are presented in parts a and b, respectively, of Figure 6. In Figure 6a, no PHBV crystallization peak is evident for the composites comprising less than 2.3 wt % CNWs. The crystallization peak appeared and became more pronounced with increasing CNW content when the content was >2.3 wt %. This result shows that there seemed to be a transition in PHBV crystallization behavior at 2.3 wt % CNW content. In Figure 6b, similar transitions in glass transition temperature, cold crystallization temperature, and melting temperatures could also be found. Neat PHBV had the lowest glass transition temperature (T_g = −5.7 °C). The addition of CNW (content ≤ 2.3 wt %) increased T_g by ca. 4 °C. At higher CNW contents (≥2.9 wt %), T_g decreased and was only ca. 1.5 °C higher than that of the neat PHBV. The cold crystallization temperature decreased with CNW content up to 2.3 wt %. Higher than that concentration, the cold crystallization temperature remained largely unchanged. In terms of melting temperatures, the samples comprising ≤2.3 wt % CNWs exhibited higher melting temperatures than those containing ≥3.3 wt % CNWs. All these thermal transitions indicated that the microstructures of the nanocomposites experienced a rapid change at about 2.3 wt % CNW concentration.

Isothermal crystallization behaviors of PHBV and PHBV/CNW composites were studied by POM (Figure 7). PHBV spherulites in the neat PHBV showed the typical Maltese cross related to crystalline structures (Figure 7a,b). The number of the spherulites was small and their diameter was large. By adding 0.5 wt % CNWs, the spherulite number dramatically increased and the radius of the spherulites decreased (Figure 7c,d).

Adding 2.3 wt % CNWs further reduced the spherulite size and increased the nucleation density of PHBV crystals (Figure 7e,f). However, 4.6 wt % CNWs did not seem to cause further reduction in the spherulite size (Figure 7g,h). This effect was previously described as a "saturation" of nucleation effect.[73] A more detailed study on the effects of CNWs on the crystallization rate, degree of crystallinity, and nucleation ability of PHBV is underway.

dx.doi.org/10.1021/ie2023367 | Ind. Eng. Chem. Res. 2012, 51, 2941−2951

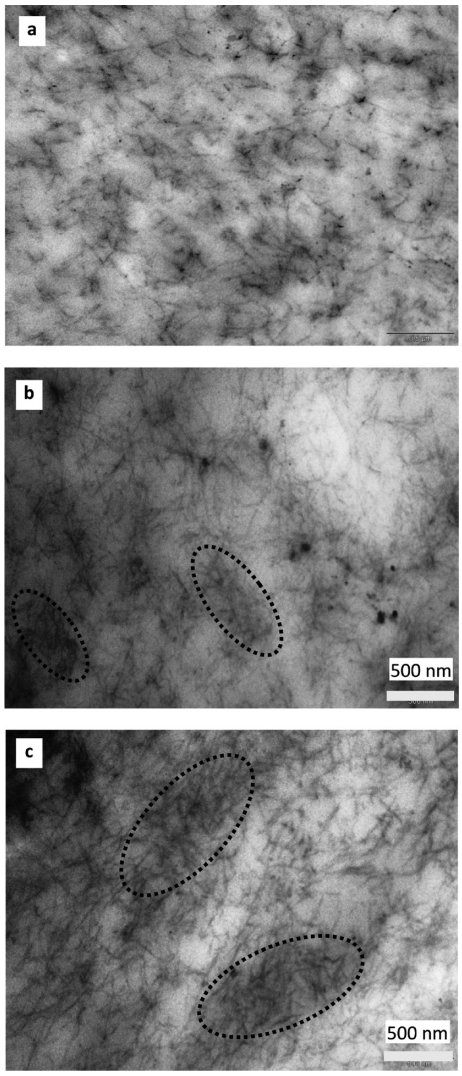

Figure 4. TEM images of PHBV/CNW composite films: (a) 2.3 wt % CNWs; (b) 3.3 wt % CNWs; (c) 4.6 wt % CNWs. The circles indicate CNW agglomerations.

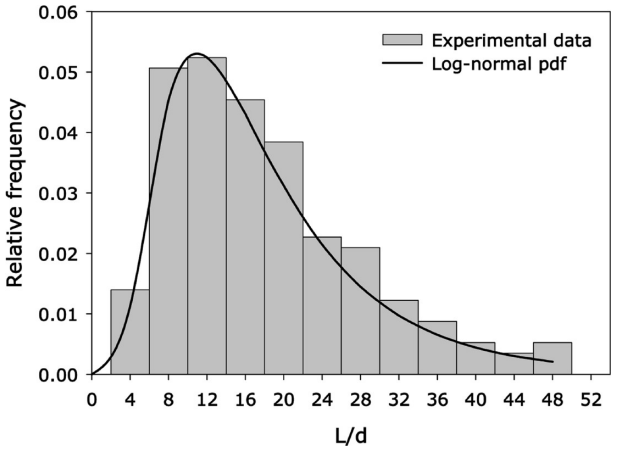

Figure 5. CNW aspect ratio distribution histograms and log-normal function fit.

Rheological Properties. Neat PHBV showed typical polymer melt behavior in the terminal region: G' and G'' increased with shear frequency ω and G'' was larger than G' (Figure 8a,b). The larger G'' indicated the fact that the PHBV melt was highly viscous rather than elastic at the test temperature. The addition of CNWs increased the G' and G'' of the composites, especially within the terminal region. G' and G'' also appeared to be more independent of shear frequency with increasing CNW content, a sign of transition from a "liquid"-like rheological behavior to a "solid"-like one. The most rapid change seemed to occur when the CNW content was between 0.5 and 2 wt %. The relative magnitude of G' and G'' also changed with increasing CNW content because G' increased faster than did G''.

Figure 8c shows that 1.2 wt % was the transitional CNW content where G' and G'' had similar values (for clarity, only the values of three formulations are shown). Below this content G' was larger than G'', whereas above this content G' was smaller than G''. This relative magnitude change indicated that the composites were dominantly elastic when the CNW content was higher than 1.2 wt %. This transition was also demonstrated by the dissipation factor tan δ (Figure 8d).

The factor was significantly reduced at 1.2 wt % CNW content, implying that the material became substantially more elastic and dissipated much less energy during shear deformation compared to the samples with lower CNW contents.

Mechanical Properties. Mechanical properties of the neat PHBV and the PHBV/CNW composite films were studied by tensile and bulge tests. Values of the Young's modulus E obtained from both methods are shown in Figure 9, and the two results are in reasonable agreement. The results from both tests indicated that the properties of the nanocomposites experienced a transition at 2.3 wt % CNWs. For the bulge test, 2.3 wt % CNWs was the concentration dividing the high modulus group (0.5, 1.2, and 2.0 wt %) and the low modulus group (2.9, 3.3, 3.6, 4.2, and 4.6 wt %). For the tensile test, 2.3 wt % CNWs was the concentration where the modulus of the composites started leveling off. Tensile strength and effective toughness (area below the stress−strain curve) were also improved by the addition of CNWs (content ≤2.3 wt %) (Figure 10). The increase in tensile strength was an indication of strong interfacial bonding between the PHBV matrix and CNWs. The improvement in toughness was due to the increase in tensile strength and elongation. Both started to decrease after the CNW content reached 2.3 wt %.

Values of the storage modulus E' of the neat polymer and the nanocomposites were measured by DMA over the temperature range −40 to 85 °C, and their representative curves are shown in Figure 11. The modulus drop between 10 and 30 °C was due to the α-relaxation of PHBV. Ten replicates were tested, and their average moduli at −10 and 60 °C, respectively, are plotted against CNW content in Figure 12. Again, a modulus transition is evident at the CNW content of 2.3−2.9 wt %. The glass transition temperature T_g of the composites (indicated by the peak of tan δ curves) was shifted to higher temperatures due to restrained mobility of PHBV chains (figure not shown). The detailed influence of CNWs on the T_g of PHBV was discussed previously in ref 63.

Dielectric Properties. Permittivity is an indicator of a material's ability to transmit an electric field. It is determined by the ability of a material to polarize in response to the applied field. Due to its frequency dependence, the permittivity of a material is often represented by the complex permittivity ε^*:

$$\varepsilon^* = \varepsilon' - i\varepsilon'' \quad (6)$$

dx.doi.org/10.1021/ie2023367 | Ind. Eng. Chem. Res. 2012, 51, 2941−2951

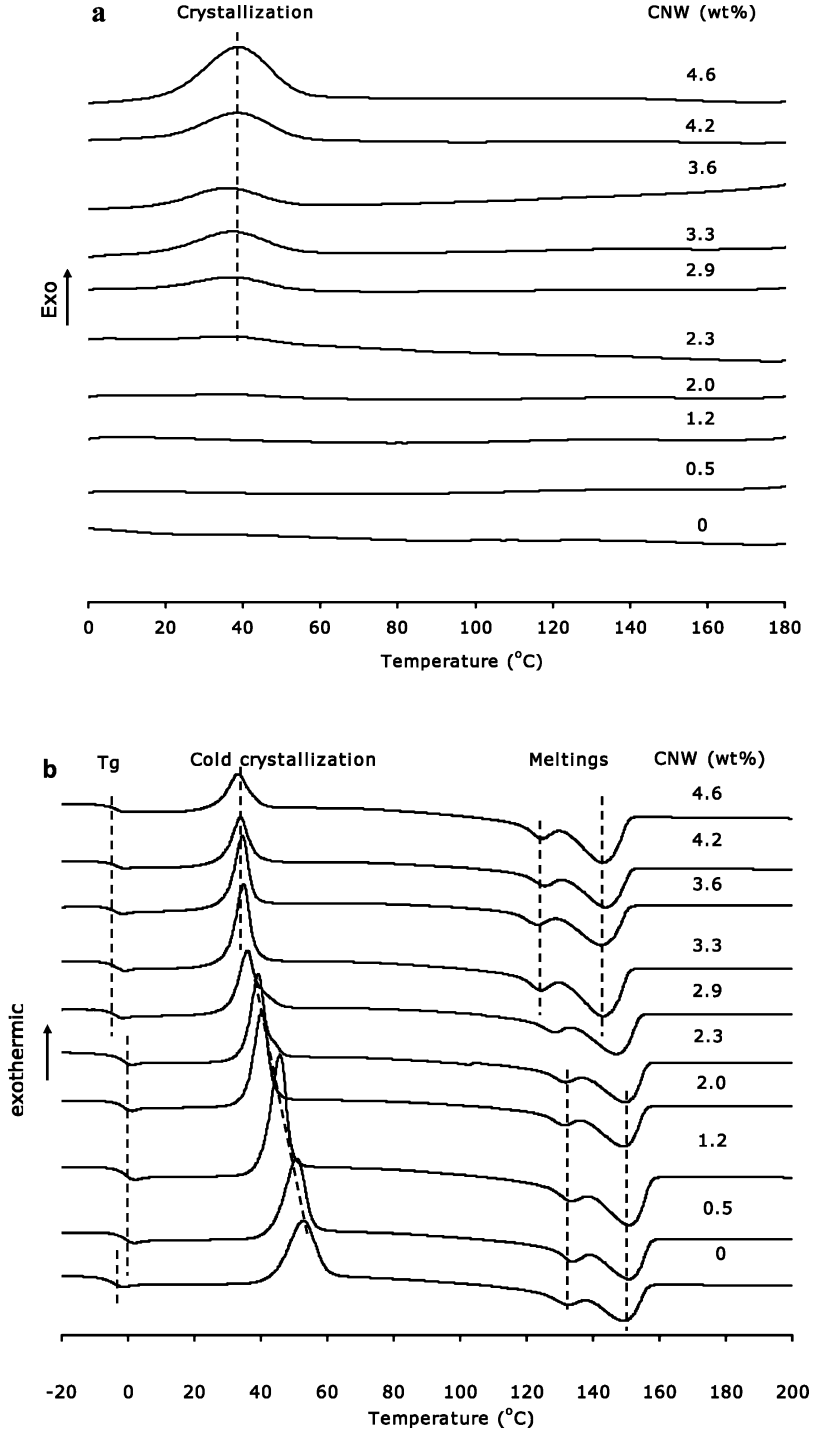

Figure 6. DSC thermograms of (a) the first cooling scan and (b) the second heating scan of the neat PHBV and the PHBV/CNW composites.

where ε' is the real part or dielectric constant and ε'' is the imaginary part of the dielectric permittivity. The specific conductivity is related to the dielectric constant by

$$\sigma^* = 2\pi i f \varepsilon_0(\varepsilon^* - 1) = \sigma' - i\sigma'' \quad (7)$$

where f is the frequency (Hz), ε_0 is the vacuum permittivity (8.85×10^{-12} F/m), and σ' and σ'' are the real and imaginary parts of the electric conductivity, respectively. The dielectric constant for a polymer depends on the polarizability of its molecules. High molecular polarizability leads to high ε^*. As a heterogeneous system, a composite also has its dielectric properties influenced by interfacial polarization, i.e., charge buildup at the interfaces.

Figure 13 compares the real permittivity ε' of the neat PHBV and the PHBV/CNW composites in the electric field with a frequency range of 10^{-2}–10^{6} Hz. ε' increased with CNW concentration and peaked at 2.3 wt %. It decreased when the concentration increased further. Figure 13 also shows that ε' of

dx.doi.org/10.1021/ie2023367 | Ind. Eng. Chem. Res. 2012, 51, 2941–2951

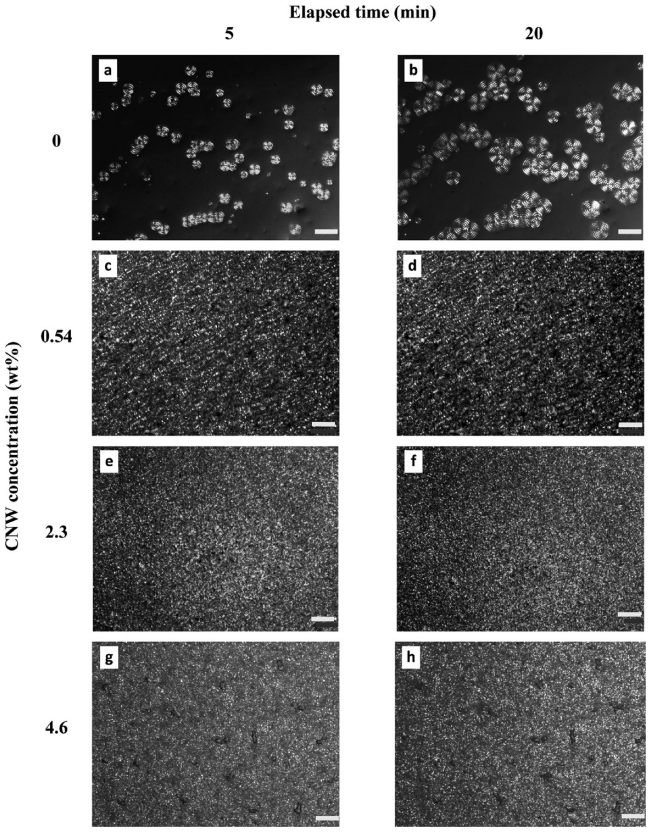

Figure 7. POM images of isothermal crystallization of neat PHBV (a,b), PHBV/0.54% CNWs (c,d), PHBV/2.3% CNWs (e,f), and PHBV/4.6% CNWs (g,h). Elapsed time was 5 (a,c,e,g) and 20 min (b,d,f,h). Scale bar represents 20 μm.

all the samples decreased with increasing frequency. This could be attributed to the relatively slow rotation and motion of the dipoles in the material, which was not able to follow the applied electric field at high frequencies.

The dependence of ε' on CNW concentration is better shown in Figure 14a, where ε' values of all the samples are compared at 1 Hz. Figure 14a clearly shows that ε' peaks at 2.3% CNW concentration. Specific conductivity of the composites, by contrast, increased monotonically with increasing CNW content (Figure 14b).

DISCUSSION

The morphology, thermal and crystallization, and mechanical and dielectric properties of the PHBV/CNW composites showed transitions at the CNW content of 2.3 wt %. Strength, modulus, and real permittivity of the composites all increased with increasing CNW content before they peaked at 2.3 wt %. Abrupt property increases of composites are often explained using the percolation theory, i.e., the formation of a long-range network structure. A percolation threshold υ_{RC} of nanoparticles can be calculated by

$$\upsilon_{RC} = \frac{0.7}{L/D} \tag{8}$$

where υ_{RC} is the minimum volume ratio for the nanoparticles to form a continuous network within a polymer matrix and L and D are the particle length and diameter, respectively.[65−70,74,75] Based on this equation, the percolation threshold of CNWs was calculated to be 3.8 vol % using the CNW aspect ratio of 18. Given the densities of PHBV (1.2 g/cm^3) and CNWs (1.5 g/cm^3),[76,77] the percolation threshold in weight ratio was 4.7 wt %. This result shows that the increases in the composite properties were not caused by CNW percolation. Rather, the continuous increases are the results of homogeneous dispersion of the CNWs and the strong interactions between PHBV and the CNWs. The decreases in the properties above the 2.3 wt % concentration was believed to be induced by CNW agglomeration as revealed in Figure 4.

In Figure 6b the cold crystallization temperature decreased until the CNW content reached 2.3 wt %. Higher than that, the temperature remained largely unchanged. CNWs facilitated PHBV cold crystallization by acting as nucleation agents. Below the CNW agglomeration content, higher CNW concentration meant larger interfacial area and more nucleation sites, which could improve PHBV cold crystallization. Above the content, the number of the nucleation sites might not increase further due to the agglomeration. The nucleation effect of CNWs might also saturate at high CNW contents. Therefore, the cold crystallization temperature did not decrease further. Moreover, it was also believed that above the CNW agglomeration content, excessive CNWs in the composites could retard PHBV crystal growth (noncrystallizable barriers)[78] and hinder the diffusion of PHBV chains to the growing crystallites.[79] In either case the perfection of PHBV crystallites was reduced and the melting point of PHBV was lowered (Figure 6b).

Rheological results are often used to indicate the formation of an interconnected network structure in polymer melts. The results in this study show that 1.2 wt % should be the transition content, which is lower than the value determined by other methods. Potschke et al.[80] found similar results in polycarbonate/multiwalled carbon nanotube (MWCNT) composites. The gelation concentration of the composites determined by rheological measurement was lower than that determined by dielectric measurement. The reason was attributed to the polymer−nanotube network structure in the rheological tests which was formed without physical touching or geometrically overlapping between nanotubes. When two nanotubes were close enough, e.g., their gap distance was lower than twice the radius of gyration of the polymer chains, such a polymer−nanotube network could be formed. The required nanotube concentration for the formation of this network was substantially lower than that required by geometrical percolation as determined by dielectric, mechanical, and thermal tests.

The tensile strength, toughness, and storage modulus of the composites all achieved their maximum values at 2.3 wt % CNW content (Figures 10−12). The CNW agglomerates which occurred at higher contents introduced stress concentration and material defects into the samples, which in turn led to lower mechanical properties.

The real permittivity of the composites peaked at 2.3 wt % CNWs (Figure 14a). The conductivity of the composites, on the other hand, increased monotonically (Figure 14b). PHBV molecules possessed low polarity and therefore the neat polymer showed lower permittivity compared to the composites due to the presence of polar groups such as hydroxyls and sulfates on CNWs. The increase in permittivity could also be partially ascribed to the interfacial polarization that occurred at the interface between PHBV and CNWs. Interfacial polarization occurs between materials of different dielectric constants and conductivities.[74] The interfacial area

dx.doi.org/10.1021/ie2023367 | Ind. Eng. Chem. Res. 2012, 51, 2941−2951

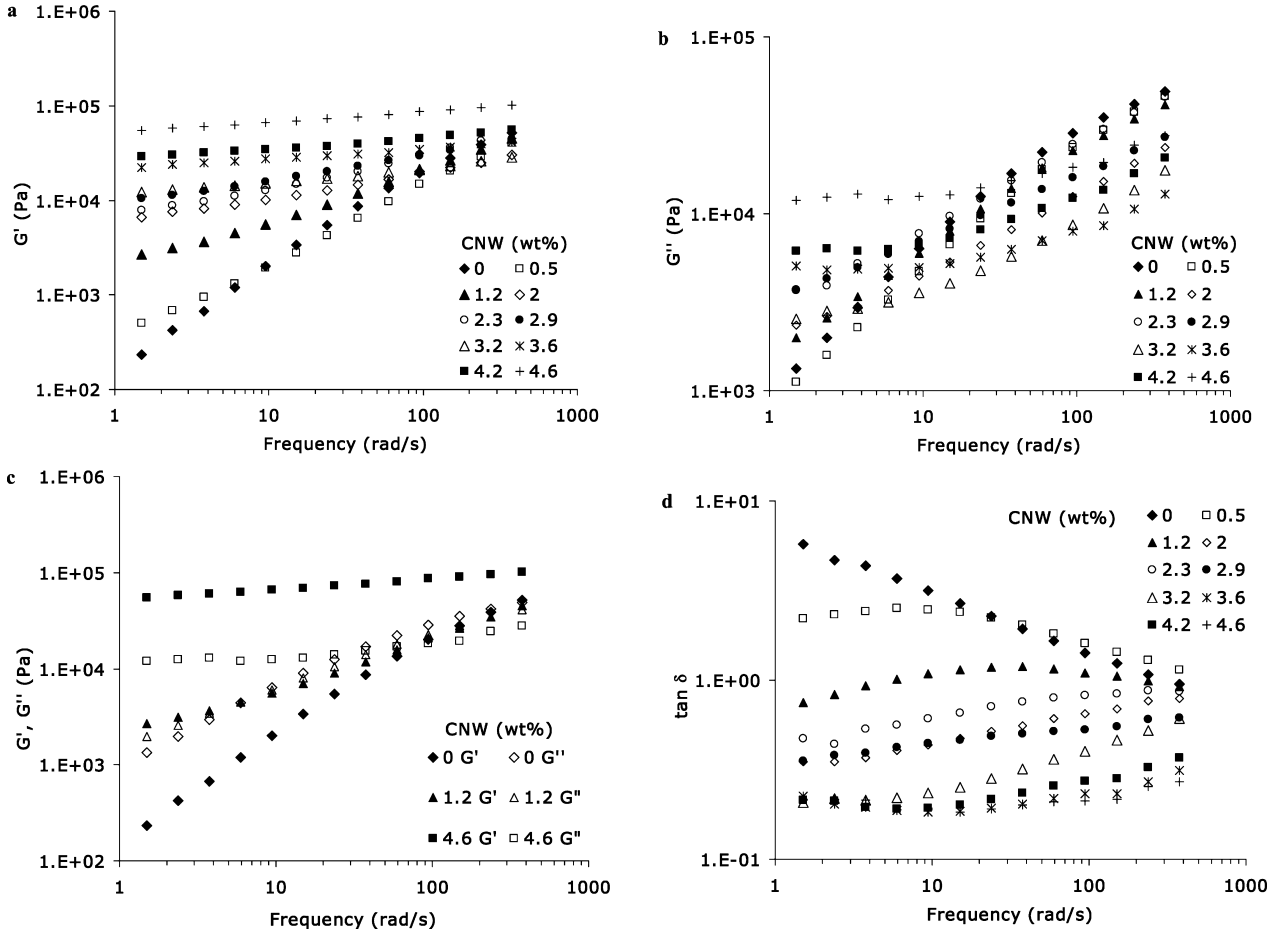

Figure 8. Storage modulus (a), loss modulus (b), storage/loss modulus (c), and dissipation factor (d) of neat PHBV and PHBV/CNW composites.

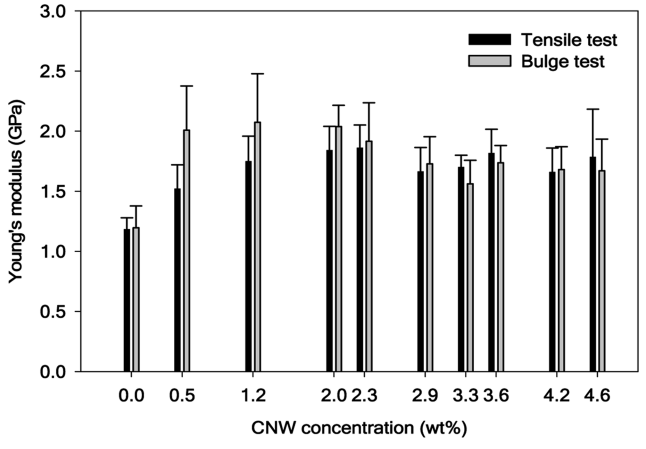

Figure 9. Young's modulus E for neat PHBV and PHBV/CNW composites obtained from tensile and bulge tests.

between PHBV and CNWs increased with CNW concentration. This resulted in increased ε' when the concentration varied from 0 to 2.3 wt %. However, above 2.3 wt % ε' started to decrease because of the reduced number of interfaces due to poor dispersion of CNWs (Figure 4). The variation of the real permittivity was believed to be due to the change in interfacial polarization. When CNW content increased from 0 to 2.3%, interconnections between CNWs and the interfacial area

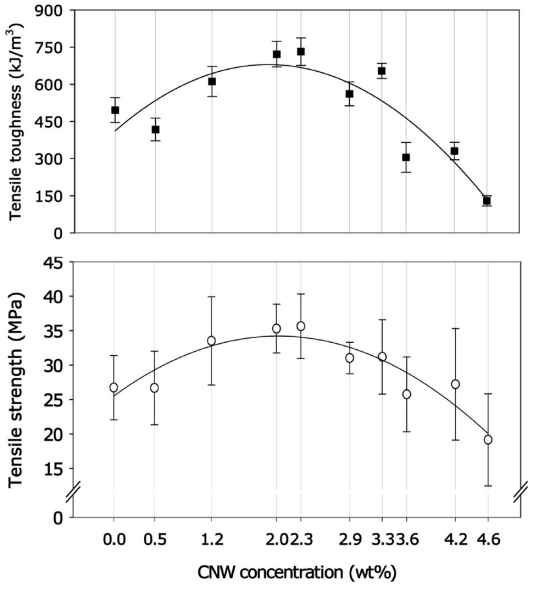

Figure 10. Tensile strength and toughness of neat PHBV and PHBV/CNW composites.

between PHBV and CNWs increased. This increase led to higher interfacial polarization and consequently higher real permittivity. However, when the content was higher than 2.3 wt %,

dx.doi.org/10.1021/ie2023367 | Ind. Eng. Chem. Res. 2012, 51, 2941−2951

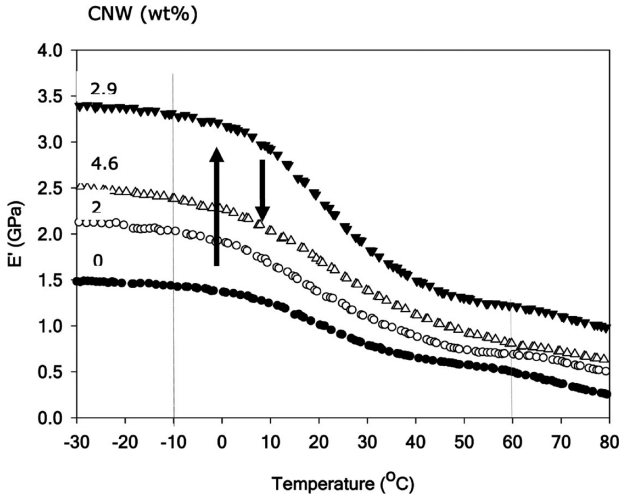

Figure 11. Storage modulus E' as a function of temperature for PHBV/CNW composites with different CNW contents.

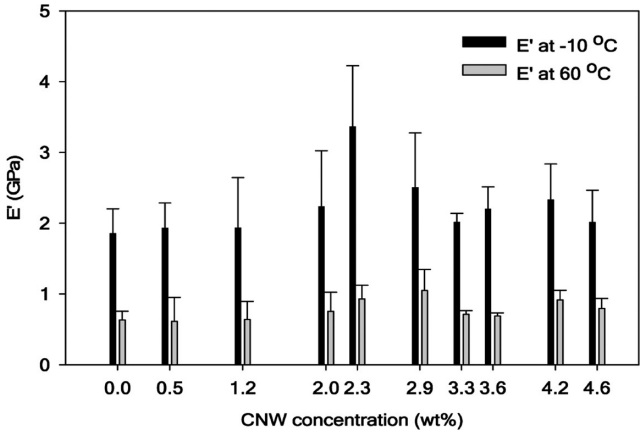

Figure 12. Storage modulus E' for neat PHBV and PHBV/CNW composites at −10 and 60 °C, respectively.

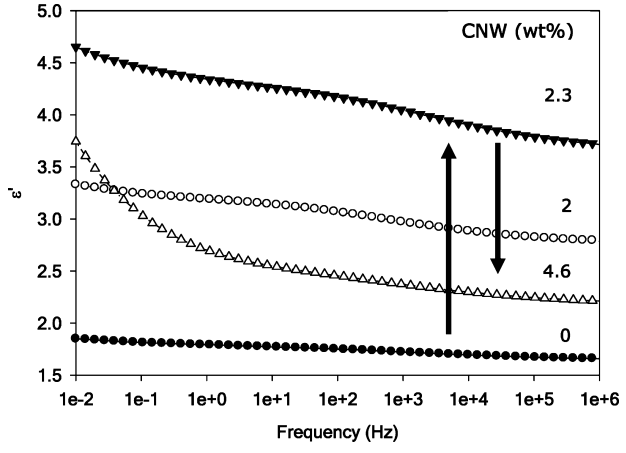

Figure 13. Real permittivity of neat PHBV and PHBV/CNW composites at room temperature in electric fields of different frequencies.

CNW agglomeration could reduce the interconnections and the interfacial area and therefore decrease the real permittivity. In addition, high conductivity of the composites at high CNW contents (>2.3 wt %) could also reduce the permittivity.

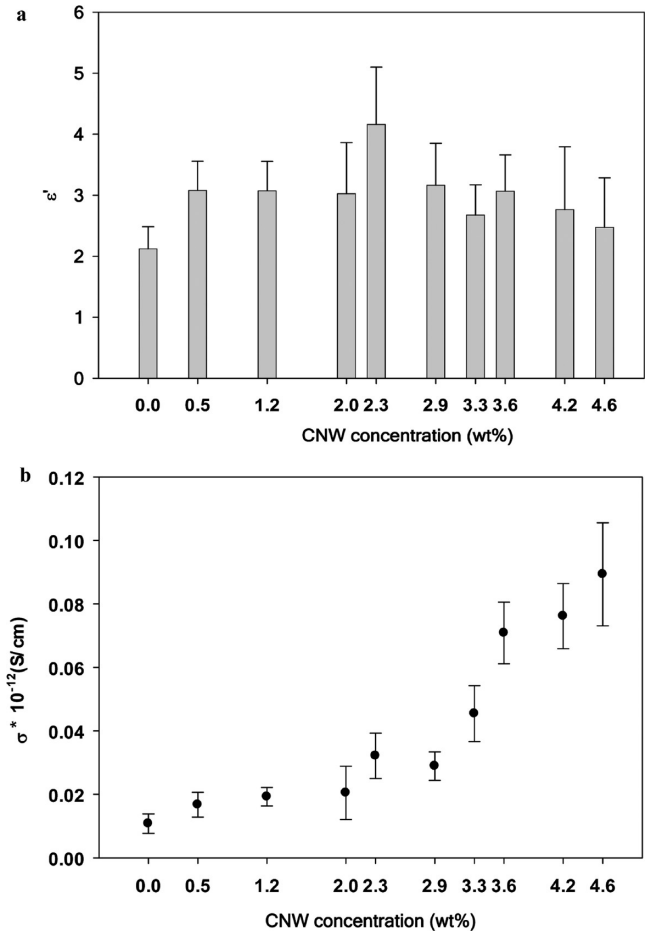

Figure 14. Real permittivity (a) and real conductivity (b) for neat PHBV and PHBV/CNW composites. ε' and σ^* were sampled at 1 Hz.

CONCLUSION

PHBV/CNW nanocomposites were prepared by solvent exchange and solution casting techniques. CNW content in the composites was varied and its effects on the morphological, mechanical, thermal, electrical, and rheological properties of the composites were investigated. Property transitions were noticed at the CNW content of 2.3 wt % for all the investigated properties except the rheological properties. These property transitions were believed to be due to the transition of the CNW dispersion state, i.e., from homogeneous dispersion to agglomeration. Rheological results indicated a lower transition point (1.2 wt %) for the composites because a polymer−CNW network could be formed without physical touching and geometrical overlapping. The calculation for the percolation threshold revealed that CNW agglomeration occurred before a percolation network was formed. This could be due to the strong interactions (e.g., hydrogen bonding) between the CNWs and their relatively low aspect ratio.

AUTHOR INFORMATION

Corresponding Author

*E-mail: wolcott@wsu.edu (M.P.W.) or long.jiang@ndsu.edu (L.J.).

dx.doi.org/10.1021/ie2023367 | Ind. Eng. Chem. Res. 2012, 51, 2941−2951

REFERENCES

(1) Sakurada, I.; Nukushina, Y.; Ito, T. Experimental determination of the elastic modulus of crystalline regions in oriented polymers. *J. Polym. Sci.* **1962**, *57*, 651.

(2) Matsuo, M.; Sawatari, C.; Iwai, Y.; Ozaki, F. Effect of orientation distribution and crystallinity on the measurement by X-ray diffraction of the crystal lattice moduli of cellulose I and II. *Macromolecules* **1990**, *23* (13), 3266.

(3) Stucova, A.; Davies, G.; Eichhorn, S. J. The Elastic Modulus and Stress-Transfer Properties of Tunicate Cellulose Whiskers. *Biomacromolecules* **2005**, *6*, 1055.

(4) Bondeson, D.; Mathew, A.; Oksman, K. Optimization of the isolation of nanocrystals from microcrystalline cellulose by acid hydrolysis. *Cellulose* **2006**, *13*, 171.

(5) Rusli, R.; Eichhorn, S. J. Determination of the Stiffness of Cellulose Nanowhiskers and the Fibre-Matrix Interface in a Nanocomposite Using Raman Spectroscopy. *Appl. Phys. Lett.* **2008**, *93*, 033111.

(6) Bondeson, D.; Kvien, I. Oksman, K. Strategies for preparation of cellulose whiskers from microcrystalline cellulose as reinforcement in nanocomposites. In *Cellulose Nanocomposites Processing: Characterization and Properties*; Oksman, K., Mohini, S., Eds.; ACS Symposium Series 938; Oxford University Press: New York, 2006; pp 11−25.

(7) Kvien, I.; Oksman, K. Orientation of cellulose nanowhiskers in polyvinyl alcohol. *Appl. Phys. A: Mater. Sci. Process.* **2007**, *87*, 641.

(8) Roohani, M.; Habibi, Y.; Belgacem, N. M.; Ebrahim, G.; Karimi, A. N.; Dufresne, A. Cellulose whiskers reinforced polyvinyl alcohol copolymers nanocomposites. *Eur. Polym. J.* **2008**, *44*, 2489.

(9) Paralikar, S. A.; Simonsen, J.; Lombardi, J. Poly(vinyl alcohol)/cellulose nanocrystal barrier membranes. *J. Membr. Sci.* **2008**, *320*, 248.

(10) Wang, Y.; Chang, C.; Zhang, L. Effects of freezing/thawing cycles and cellulose nanowhiskers on structure and properties of biocompatible starch/PVA sponges. *Macromol. Mater. Eng.* **2010**, *295*, 137.

(11) Goetz, L.; Mathew, A.; Oksman, K.; Gatenholm, P.; Ragauskas, A. A novel nanocomposite film prepared from crosslinked cellulosic whiskers. *Carbohydr. Polym.* **2009**, *75*, 85.

(12) Ibnyaich, A. M.S. Thesis, Luleå University of Technology, Luleå, Sweden, 2010.

(13) Favier, V.; Chanzy, H.; Cavaille, J. Y. Polymer nanocomposites reinforced by cellulose whiskers. *Macromolecules* **1995**, *28* (18), 6365.

(14) Helbert, W.; Cavaille, J. Y.; Dufresne, A. Thermoplastic nanocomposites filled with wheat straw cellulose whiskers. Part I: processing and mechanical behavior. *Polym. Compos.* **1996**, *17*, 604.

(15) Hajji, P.; Cavaille, J. Y.; Favier, V.; Gauthier, C.; Vigier, G. Tensile behavior of nanocomposies from latex and cellulose whiskers. *Polym. Compos.* **1996**, *4*, 612.

(16) Azizi Samir, M.; Alloin, F.; Paillet, M.; Dufresne, A. Tangling effect in fibrillated cellulose reinforced nanocomposites. *Macromolecules* **2004**, *37*, 4313.

(17) Elmabrouk, A. B.; Wim, T.; Dufresne, A.; Boufi, S. Preparation of poly(styrene-co-hexylacrylate)/cellulose whiskers nanocomposites via miniemulsion polymerization. *J. Appl. Polym. Sci.* **2009**, *114*, 2946.

(18) Anglès, M.; Dufresne, A. Plasticized starch/tunicin whiskers nanocomposite materials 2. Mechanical behavior. *Macromolecules* **2001**, *34*, 2921.

(19) Mathew, A.; Dufresne, A. Morphological investigation of nanocomposites from sorbitol plasticized starch and tunicin whiskers. *Biomacromolecules* **2002**, *3*, 609.

(20) Kvien, I.; Sugiyama, J.; Votrubec, M.; Oksman, K. Characterization of starch based nanocomposites. *J. Mater. Sci.* **2007**, *42*, 8163.

(21) Chen, Y.; Liu, C.; Chang, P.; Cao, X.; Anderson, D. Bionanocomposites based on pea starch and cellulose nanowhiskers hydrolyzed from pea hull fibre: Effect of hydrolysis time. *Carbohydr. Polym.* **2009**, *76*, 607.

(22) García, N. L.; Ribba, L.; Dufresne, A.; Aranguren, M. I.; Goyanes, S. Physico-mechanical properties of biodegradable starch nanocomposites. *Macromol. Mater. Eng.* **2009**, *294*, 169.

(23) Anglès, M. N.; Dufresne, A. Plasticized/tunicin Whiskers Nanocomposites Materials. 1. Structural analysis. *Macromolecules* **2000**, *33*, 8344.

(24) de M. Teixeira, E.; Pasquini, D.; Curvelo, A. S.; Corradini, E.; Belgacem, M. N.; Dufresne, A. Cassava bagasse whiskers reinforced plasticized cassava starch. *Carbohydr. Polym.* **2009**, *78*, 422.

(25) Azizi Samir, M.; Alloin, F.; Sanchez, J.; Dufresne, A. Cellulose nanocrystals reinforced poly(oxyethylene). *Polymer* **2004**, *45* (12), 4149.

(26) Azizi Samir, M.; Alloin, F.; Sanchez, J.-Y.; Dufresne, A. Nanocomposite polymer electrolytes based on Poly(oxyethylene) and cellulose whiskers. *Polim.: Cienc. Tecnol.* **2005**, *15*, 109.

(27) Nair, K. G.; Dufresne, A. Crab Shell Chitin Whisker Reinforced Natural Rubber Nanocomposites. 1. Processing and Swelling Behavior. *Biomacromolecules* **2003**, *4*, 657.

(28) Nair, K. G.; Dufresne, A. Crab shell chitin whisker reinforced natural rubber nanocomposites. 2. Mechanical behavior. *Biomacromolecules* **2003**, *4*, 666.

(29) Nair, K. G.; Dufresne, A. Crab shell chitin whiskers reinforced natural rubber nanocomposites. 3. Effect of chemical modification of chitin whiskers. *Biomacromolecules* **2003**, *4*, 1835.

(30) Angellier, H.; Molina-Boisseau, S.; Dufresne, A. Mechanical properties of waxy maize starch nanocrystals reinforced natural rubber. *Macromolecules* **2005**, *38*, 9161.

(31) Wang, Y.; Cao, X.; Zhang, L. Effects of Cellulose Whiskers on Properties of Soy Protein Thermoplastics. *Macromol. Biosci.* **2006**, *6*, 524.

(32) Zheng, H.; Ai, F.; Chang, P. R.; Huang, J.; Dufresne, A. Structure and Properties of Starch Nanocrystal-Reinforced Soy Protein Plastics. *Polym. Compos.* **2009**, *30*, 474.

(33) Pasquini, D.; de Morais Teixeira, E.; da Silva Curvelo, A. A.; Belgacem, M. N.; Dufresne, A. Surface esterification of cellulose fibres: Processing and characterisation of low-density polyethylene/cellulose fibres composites. *Compos. Sci. Technol.* **2008**, *68*, 193.

(34) Habibi, Y.; El-Zawawy, W. K.; Ibrahim, M. M.; Dufresne, A. Processing and characterization of reinforced polyethylene composites made with lignocellulosic fibers from Egyptian agro-industrial residues. *Compos. Sci. Technol.* **2008**, *68*, 1877.

(35) de Menezes, A. J.; Siqueira, G.; Curvelo, A.; Dufresne, A. Extrusion and characterization of functionalized cellulose whisker reinforced polyethylene Nanocomposites. *Polymer* **2009**, *50*, 4552.

(36) Ljungberg, N.; Bonini, C.; Bortolussi, F.; Boisson, C.; Heux, L.; Cavaille, J. Y. New nanocomposite materials reinforced with cellulose whiskers in atactic polypropylene: Effect of surface and dispersion characteristics. *Macromolecules* **2005**, *6*, 2732.

(37) Ljungberg, N.; Cavaille, J. Y.; Heux, L. Nanocomposites of isotactic polypropylene reinforced with rod-like cellulose whiskers. *Polymer* **2006**, *47*, 6285.

(38) Chazeau, L; Cavaille, J. Y.; Ganova, G.; Dendievel, R.; Boutherin, B. Viscoelastic properties of plasticized PVC reinforced with cellulose whiskers. *J. Appl. Polym. Sci.* **1999**, *71*, 1797.

(39) de Rodriguez, N.; Thielemans, W.; Dufresne, A. Sisal cellulose whiskers reinforced polyvinyl acetate nanocomposites. *Cellulose* **2006**, *13*, 261.

(40) Siqueira, G.; Bras, J.; Dufresne, A. Cellulose whiskers versus microfibrils: influence of the nature of the nanoparticle and its surface functionalization on the thermal and mechanical properties of nanocomposites. *Biomacromolecules* **2009**, *10*, 425.

(41) Mathew, A.; Oksman, K.; Sain, M. Mechanical properties of biodegradable composites from poly lactic acid (PLA) and microcrystalline cellulose (MCC). *J. Appl. Polym. Sci.* **2005**, *97*, 2014.

(42) Oksman, K.; Mathew, A.; Bondeson, D.; Kvien, I. Manufacturing process of polylactic acid (PLA)-cellulose whiskers nanocomposites. *Compos. Sci. Technol.* **2006**, *66*, 2776.

(43) Bondeson, D.; Oksman, K. Polylactic acid/cellulose whisker nanocomposites modified by polyvinyl alcohol. *Composites, Part A* **2007**, *38*, 2486.

(44) Lin, N.; Chen, G.; Huang, J.; Dufresne, A.; Chang, P. R. Effects of polymer-grafted natural nanocrystal on structure and mechanical

properties of poly(lactic acid): a case of cellulose whisker-graft-polycaprolactone. *J. Appl. Polym. Sci.* **2009**, *113*, 3417.
(45) Yu, J.; Ai, F.; Dufresne, A.; Gao, S.; Huang, J.; Chang, P. R. Structure and mechanical properties of poly(lactic acid) filled with (starch nanocrystal)-graft-poly(ε-caprolactone). *Macromol. Mater. Eng.* **2008**, *293*, 763.
(46) Pandey, J. K.; Chu, W. S.; Kim, S. C.; Lee, C. S.; Ahn, S. H. Bio-nano reinforcement of environmentally degradable polymer matrix by cellulose whiskers from grass. *Composites, Part B* **2009**, *40*, 676.
(47) Sanchez-Garcia, M. D.; Lagaron, J. M. On the use of plant cellulose nanowhiskers to enhance the barrier properties of polylactic acid. *Cellulose* **2010**, *17*, 987.
(48) Pei, A.; Zhou, Q.; Berglund, L. A. Functionalized cellulose nanocrystals as biobased nucleation agents in poly(L-lactide) (PLLA)——Crystallization and mechanical property effects. *Compos. Sci. Technol.* **2010**, *70*, 815.
(49) Vargas, N. H. M.S. Thesis, Luleå University of Technology, Luleå, Sweden, 2010.
(50) Dufresne, A.; Kellerhals, M. B.; Witholt, B. Transcrystallization in Mcl-PHAs/cellulose whiskers composites. *Macromolecules* **1999**, *32*, 7396.
(51) Petersson, L.; Mathew, A. P.; Oksman, K. Dispersion and properties of cellulose nanowhiskers and layered silicates in cellulose acetate butyrate nanocomposites. *J. Appl. Polym. Sci.* **2009**, *112*, 2001.
(52) Grunert, M.; Winter, W. T. Nanocomposites of cellulose acetate butyrate reinforced with cellulose nanocrystals. *J. Polym. Environ.* **2002**, *10*, 27.
(53) Petersson, L.; Oksman, K. Optimization of the preparation of nano crystals from microcrystalline cellulose in aqueous suspensions In *Abstracts of Papers*, 229th National Meeting of the American Chemical Society, San Diego, CA, US, March 13−17, 2005; American Chemical Society: Washington, DC, 2005.
(54) Ayuk, J. E.; Mathew, A. P.; Oksman, K. The effect of plasticizer and cellulose nanowhisker content on the dispersion and properties of cellulose acetate butyrate nanocomposites. *J. Appl. Polym. Sci.* **2009**, *114*, 2723.
(55) Cao, X.; Dong, H.; Li, C. New nanocomposite materials reinforced with flax cellulose nanocrystals in waterborne polyurethane. *Biomacromolecules* **2007**, *8*, 899.
(56) Cao, X.; Chang, P. R.; Huneault, M. A. Preparation and properties of plasticized starch modified with poly(ε-caprolactone) based waterborne polyurethane. *Carbohydr. Polym.* **2008**, *71*, 119.
(57) Chen, G.; Wei, M.; Chen, J.; Huang, J.; Dufresne, A.; Chang, P. R. Simultaneous Reinforcing and Toughening: New Nanocomposites of Waterborne Polyurethane Filled with Low Loading Level of Starch Nanocrystals. *Polymer* **2008**, *49*, 1860.
(58) Chang, P. R.; Ai, F.; Chen, Y.; Dufresne, A.; Huang, J. Effects of starch nanocrystals-graft-polycaprolactone on mechanical properties of waterborne polyurethane-based nanocomposites. *J. Appl. Polym. Sci.* **2009**, *111*, 619.
(59) Ruiz, M.; Cavaille, J. Y.; Dufresne, A.; Gerard, J. F.; Graillat, C. Processing and characterization of new thermoset nanocomposites based on cellulose whiskers. *Compos. Interfaces* **2000**, *7*, 117.
(60) Ruiz, M.; Cavaille, J. Y.; Dufresne, A.; Granillat, C.; Gerard, J. New waterborne epoxy coatings based on cellulose nanofillers. *Macromol. Symp.* **2001**, *169*, 211.
(61) Abdelmouleh, M.; Boufi, S.; Belgacem, M. N.; Dufresne, A.; Gandini, A. Modification of cellulose fibers with functionalized silanes: Effect of the fiber treatment on the mechanical performances of cellulose−thermoset composites. *J. Appl. Polym. Sci.* **2005**, *98*, 974.
(62) Jiang, L.; Morelius, E.; Zhang, J.; Wolcott, M. P.; Holbery, J. Study of the poly(3-hydroxybutyrate-co-3-hydroxyvalerate)/cellulose nanowhisker composites prepared by solution casting and melt processing. *J. Compos. Mater.* **2008**, *42*, 2629.
(63) Ten, E.; Turtle, J.; Barh, D.; Jiang, L.; Wolcott, M. P. Thermal and mechanical properties of poly(3-hydroxybutyrate-co-3-hydroxyvalerate)/cellulose nanowhiskers composites. *Polymer* **2010**, *51*, 2652.
(64) Flandin, L.; Bidan, G.; Bréchet, Y.; Cavaillé, J. Y. New nanocomposite materials made of an insulating matrix and conducting fillers: processing and properties. *Polym. Compos.* **2000**, *21* (2), 165.
(65) Azizi Samir, M.; Alloin, F.; Dufresne, A. A review of recent research into cellulosic whiskers, their properties and their application in nanocomposite field. *Biomacromolecules* **2005**, *6*, 612.
(66) Dufresne, A. Polysaccharide nano crystal reinforced nanocomposites. *Can. J. Chem.* **2008**, *86*, 484.
(67) Eichhorn, S. J.; Dufresne, A.; Aranguren, M.; Marcovich, N. E.; Capadona, J. R.; Rowan, S. J.; Weder, C.; Thielemans, W.; Roman, M.; Renneckar, S.; Gindl, W.; Veigel, S.; Keckes, J.; Yano, H.; Abe, K.; Nogi, M.; Nakagaito, A. N.; Mangalam, A.; Simonsen, J.; Benight, A. S.; Bismarck, A.; Berglund, L. A.; Peijs, T. Review: current international research into cellulose nanofibers and nanocomposites. *J. Mater. Sci.* **2010**, *45*, 1.
(68) Siqueira, G.; Bras, J.; Dufresne, A. Cellulosic Bionanocomposites: A Review of Preparation, Properties and Applications. *Polymers* **2010**, *2*, 728.
(69) Habibi, Y.; Lucia, L. A.; Rojas, O. J. Cellulose nanocrystals: Chemistry, self-assembly, and applications. *Chem. Rev.* **2010**, *110* (6), 3479.
(70) Moon, R.; Martini, A.; Nairn, J.; Simonsen, J.; Youngblood, J. Cellulose nanomaterials review: structure, properties and nanocomposites. *Chem. Soc. Rev.* **2011**, *40*, 3941.
(71) Di Lorenzo, M.; Sajkiewicz, P.; Gradys, A.; La Pietra, P. Optimization of melting conditions for the analysis of crystallization kinetics of poly(3-hydroxybutyrate). *e-Polym.* **2009**, No. no. 027.
(72) Small, M.; Nix, W. J. Analysis of the accuracy of the bulge test in determining the mechanical properties of thin films. *J. Mater. Res.* **1992**, *7*, 1553.
(73) Xu, D.; Wang, Z. Role of multi-wall carbon nanotube network in composites to crystallization of isotactic polypropylene matrix. *Polymer* **2008**, *49*, 330.
(74) Paul, A.; Thomas, S. Electrical properties of natural-fiber-reinforced low density polyethylene composites: A comparison with carbon black and glass-fiber-filled low density polyethylene composites. *J. Appl. Polym. Sci.* **1997**, *63* (2), 247.
(75) Favier, V. Etude de nouveaux matériaux composites obtenus à partir de latex filmogènes et de whiskers de cellulose: effet de percolation mécanique. Ph.D. Thesis, Joseph Fourier University, Grenoble, France, 1995.
(76) Holmes, P. A. *Developments in Crystalline Polymers*; Basset, D. C., Ed.; Elsevier: London, 1987; p 1.
(77) Gindl, W.; Keckes, J. Tensile properties of cellulose acetate butyrate composites reinforced with bacterial cellulose. *Compos. Sci. Technol.* **2004**, *64*, 2407.
(78) Homminga, D.; Goderis, B.; Dolbnya, I.; Reynaers, H.; Groeninckx, G. Crystallization behavior of polymer/montmorillonite nanocomposites. Part I. Intercalated poly(ethylene oxide)/montmorillonite nanocomposites. *Polymer* **2005**, *46*, 11359.
(79) Fornes, T. D.; Paul, D. R. Modeling properties of nylon 6/clay nanocomposites using composite theories. *Polymer* **2003**, *44*, 3945.
(80) Potschke, P.; Dudkin, S. M.; Alig, I. Dielectric spectroscopy on melt processed polycarbonate−multiwalled carbon nanotube composites. *Polymer* **2003**, *44*, 5023.